
**Comments on Inorganic Chemistry**
Publication details, including instructions for authors and subscription information:
http://www.informaworld.com/smpp/title~content=t713455155

# Self-Nucleated Thin Films of GaN and $Al_{x}Ga_{1-x}N$ for Optoelectronic Devices: Structure and Morphology

Thomas J. Kistenmacher[a]; Dennis K. Wickenden[a]
[a] Milton S. Eisenhower Research Center, Applied Physics Laboratory, The Johns Hopkins University, Laurel, Maryland

**To cite this Article** Kistenmacher, Thomas J. and Wickenden, Dennis K.(1996) 'Self-Nucleated Thin Films of GaN and $Al_{x}Ga_{1-x}N$ for Optoelectronic Devices: Structure and Morphology', Comments on Inorganic Chemistry, 18: 5, 325 — 341
**To link to this Article: DOI:** 10.1080/02603599608033867
**URL:** http://dx.doi.org/10.1080/02603599608033867

# Self-Nucleated Thin Films of GaN and $Al_xGa_{1-x}N$ for Optoelectronic Devices: Structure and Morphology

THOMAS J. KISTENMACHER and DENNIS K. WICKENDEN
*Milton S. Eisenhower Research Center,*
*Applied Physics Laboratory,*
*The Johns Hopkins University,*
*Laurel, Maryland 20723*

Received February 27, 1996



There is increasing interest in the use of Group IIIA nitrides (AlN, GaN, InN, and their alloys) for a variety of optoelectronic applications, including short wavelength sources and detectors. Progress, while spectacular these past few years, has been hampered by the lack of bulk, lattice-matched material to serve as the substrate for homoepitaxial growth. The most common substrate, basal plane sapphire, with a 16% lattice mismatch, requires a predeposited nucleation layer to achieve pseudo two-dimensional layer-by-layer growth suitable for device processing. The surface morphology and mosaic dispersion of both unnucleated and self-nucleated GaN thin films have been studied by a combination of real space images from atomic force and scanning tunneling microscopies and reciprocal space intensity data from X-ray scattering measurements. The unnucleated GaN films show a large-grained hexagonal relief, typical of three-dimensional island growth, while the self-nucleated films are shown to be dense mosaics of highly oriented islands emblematic of a more two-dimensional growth. High quality $Al_xGa_{1-x}N$ alloy films have also been deposited on self-nucleated sapphire substrates and exhibit minimal homogeneous and inhomogeneous strain and alloy clustering. Consistent with their reduced strain and chemical uniformity, these wide-bandgap $Al_xGa_{1-x}N$ films are suitable for a number of optoelectronic applications.

**Key Words:** *aluminum nitride, gallium nitride, metalorganic chemical vapor deposition, thin films, atomic force and scanning tunneling microscopies, X-ray diffraction, optical spectroscopy, surface structure, mosaic dispersion*

---

*Comments Inorg. Chem.*
1996, Vol. 18, Nos. 5 & 6, pp. 325–341
Reprints available directly from the publisher
Photocopying permitted by license only

## INTRODUCTION

The science and technology of semiconductors has steadily evolved from elemental devices based on Si and Ge to inorganic compound semiconductors typified by III–V (e.g., GaAs) and II–VI (e.g., ZnS, ZnSe) materials. A principal driving force for the interest in these compound semiconductors has been the desire for broad direction over the energy bandgap which ultimately allows control over the available spectral range for optical emitters and detectors and nonlinear optical elements. In conjunction with rapid progress in the control of the physical properties of semiconductors via compositional tailoring, there have been notable advances in sophisticated deposition techniques that allow for growth of homoepitaxial or heteroepitaxial layers with a thickness controlled on the atomic scale. In combination, these two advances have, for example, made possible the development of semiconducting superlattices. In particular, a compositional superlattice can be fabricated from alternate layers of different chemical formulation. The archetypal system has been the psuedobinary III–V compound Ga–Al–As. Although epilayers and superlattices based on these materials have been at the core of many useful devices (e.g., high efficiency laser diodes and infrared detectors), their relatively small bandgaps limit their technological scope.



These limitations, along with increased demands from a variety of proposed applications, has spurred renewed interest in inorganic semiconductors with wide bandgaps for the fabrication of emitters and detectors and nonlinear optical elements operable in the visible and UV bands of the electromagnetic spectrum. Particular areas of current interest for wide bandgap materials include: surface acoustic wave devices; nonlinear optical elements for frequency doubling into the ultraviolet; green-to-blue light emitters (light-emitting diodes and lasers) for communications; solar-blind detectors for UV imaging and space astronomy applications; and visible and UV lasers for reading and writing high-density recording media.

Candidate material systems include SiC, the Group II–VI semiconductors ZnS and ZnSe, and the Group IIIA nitrides. The hexagonal polytypes of SiC, although considered excellent candidates for blue light-emitting diodes and for high-temperature and high-power electronic devices, are not suitable for laser and UV applications because of their indirect and comparatively small bandgaps ($E_g \leq 3.2$ eV). Recent

progress in developing blue-green LEDs and lasers in the $ZnS_xSe_{1-x}$ alloy system has been restricted to high-selenium alloys with bandgaps < 2.8 eV. Higher-bandgap alloys continue to be plagued by autocompensation effects that preclude well-behaved conductivity control. Almost by default, then, the Group IIIA nitrides have become the preferred candidates for wavelength-selectable devices operating beyond the yellow-green region of the spectrum, and their preparation as thin films the focus of a truly worldwide research effort. Thin films of GaN and AlN have direct bandgaps of 3.4 and 6.2 eV, respectively, with corresponding cutoff wavelengths of 365 and 200 nm. Since these compounds are miscible with each other and form a complete series of aluminum gallium nitride ($Al_xGa_{1-x}N$) alloys, it should, in principle, be possible to develop optoelectronic devices tailored to operate anywhere in the indicated spectral range.



## BASICS

The isostructural nitrides of aluminum, gallium, and indium share two common crystalline motifs: the wurtzite and zinc blende structures. Under ambient conditions, the thermodynamically stable phase for GaN and its alloys with AlN is the wurtzite structure (space group $P6_3mc$, point group 6mm) depicted in Fig. 1. In that crystalline phase, each of the constituent ions is four coordinate, approximately tetrahedral, and two layers of tetrahedra define the unique **c**-axis repeat length. Moreover, as all tetrahedra are aligned head-to-tail along the **c**-axis, this unique symmetry direction is polar, and nonlinear optical signal generation is possible and potentially an important area of endeavor for optical device applications.

Moreover, in the absence of a thermodynamically stable crystalline phase to serve as a substrate for homoepitaxial growth, thin films of the Group IIIA nitrides are deposited onto foreign substrates (heteroepitaxy). In all of the studies that follow, the GaN or Al–Ga–N thin films have been grown on basal plane [denoted (00.1)] sapphire substrates. Although the chemical and crystalline structures of sapphire [$Al_2O_3$; corundum; space group $R\bar{3}c$; point group $\bar{3}m$] are quite distinct from that of the Group IIIA nitrides, the influence of symmetry and thermodynamics is such that the (00.1) plane of the nitride film parallels the (00.1) plane of the sapphire substrate. To fully characterize the heteroepitaxial

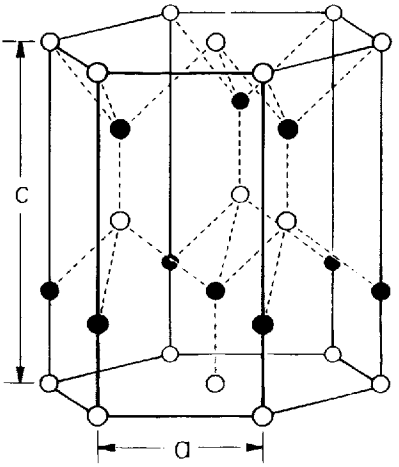


FIGURE 1 An illustration of the wurzite phase of AlN, GaN and InN.



relationship between the nitride film and the sapphire substrate, it is necessary to define the relative in-plane orientation of the a*b* nets [(hh.0) plane] of the nitride film and that of the sapphire substrate. We have typically employed the X-ray precession method[1] to ascertain the in-plane heteroepitaxial relationship for our films and find that the a*b* net for the nitride film is rotated by 30° relative to that of the sapphire substrate: $[\{10.0\}_{GaN}//\{11.0\}_{sapphire}]$. The rotation of the two lattices reduces the lattice mismatch ($a_{GaN}$ = 0.3189 nm, $a_{sapphire}$ = 0.4758 nm) between film and substrate; however, a sizable mismatch in lattice dimension and thermal expansion coefficient remains, and the associated strain along with deviations from stoichiometry are serious impediments to the realization of optimal thin films.

## GROWTH

Metalorganic chemical vapor deposition (MOCVD)[2] has emerged as one of the leading synthetic methods for thin films of GaN and its alloys. The MOCVD technique is a controlled pyrolytic process, whereby a low boiling metal organic compound [trimethylgallium, $(CH_3)_3Ga$, for example] is taken into the vapor phase by a stream of carrier gas (commonly

nitrogen or hydrogen) and combined at a heated susceptor with a reactive gas [for example, ammonia ($NH_3$)]. The hot substrate causes the precursor gases to combine at the surface following the overall reaction:

$$(CH_3)_3Ga + NH_3 \rightarrow GaN + 3CH_4.$$

This reaction leaves behind a thin film of GaN and the volatile methane is carried off in the carrier gas stream. To make materials other than GaN, it is only necessary to change the reactive gases. For example, to make a $Al_xGa_{1-x}N$ thin film, a proportional amount of trimethylaluminum is mixed with the trimethylgallium.

## GaN Thin Films

As noted earlier, the absence of an accessible, thermodynamically stable single-crystal phase to serve as a substrate for homoepitaxial deposition requires heteroepitaxial growth. Moreover, it is well known that as the lattice mismatch for heteroepitaxial systems increases, the film nucleation mechanism changes from the Frank–van der Merwe (layer-by-layer) to either the Stranski–Krastnov or Volmer–Weber (3D island) growth mode.[3] It is also becoming more widely appreciated that the use of nucleation layers can mediate the choice of growth mechanism and significantly alter dependent physical properties (as we will see shortly).

Most studies on the thin film growth of GaN have concentrated on its heteroepitaxial deposition on (00.1) sapphire substrates. The large in-plane lattice mismatch between GaN and sapphire results in three-dimensional island growth with pronounced hexagonal features. This makes it difficult to prepare device quality samples, particularly when incorporating layers containing alloys with the other Group IIIA nitrides. It has been demonstrated that the use of thin AlN buffer layers[4] significantly increases the nucleation site density for the subsequent growth of the GaN and converts the growth mechanism to pseudo-two-dimensional layer growth, resulting in the deposition of smooth, crack-free layers. Over the past several years, we and others have shown that GaN buffer layers (i.e., self-nucleation) predeposited at low growth temperatures, particularly on (00.1) oriented sapphire, greatly improve the crystallographic, electrical, and optical properties of GaN overlayers.[5,6] We have previously determined from extensive optical and X-ray measurements that GaN nucleation layers have a significant crystalline component, although the X-ray data and the lack of absorbance features near the direct bandgap of GaN suggest that the crystallites are very small and

are most probably embedded in an amorphous-like matrix. Upon annealing to higher temperatures, the crystallite size increases and the crystal perfection improves markedly, until at temperatures near those empirically determined to be optimum for growth of a heteroepitaxial overlayer, the perfection approaches that of good quality heteroepitaxial material.[7] These GaN buffer layers serve, once again, to provide a high density of sites for the nucleation of the overlayers, and such a high density of nucleation sites means that the overlayer needs to grow only a few nanometers before it coalesces and further growth proceeds by a pseudo-two-dimensional layer-by-layer mechanism.

## Atomic Force Microscopy: Surface Imaging

As expected for three-dimensional island growth,[3] deposition of GaN onto unnucleated (00.1) sapphire yields large hexagonal prisms (Fig. 2), employing either hydrogen or nitrogen as the carrier gas. In the films grown in hydrogen, Fig. 2 (A), atomic force microscopy (AFM) shows[8] that these prisms range from 50 to 100 μm in diameter, with a mean value clustered about 60–70 μm. Moreover, these prism are typically 1.5 to > 4 μm in height, but many are outside the maximum vertical and horizontal scan limits (4.5 μm × 120 μm) of the atomic force microscope. Smaller subunits on prismatic faces appear to be layered (like stacked sand dollars), with an average height of tens of nm and on average about 400 nm across.

Unnucleated films grown in nitrogen as the carrier gas also exhibit [Fig. 2 (B)] large hexagonal prisms, but in this case the prisms have base

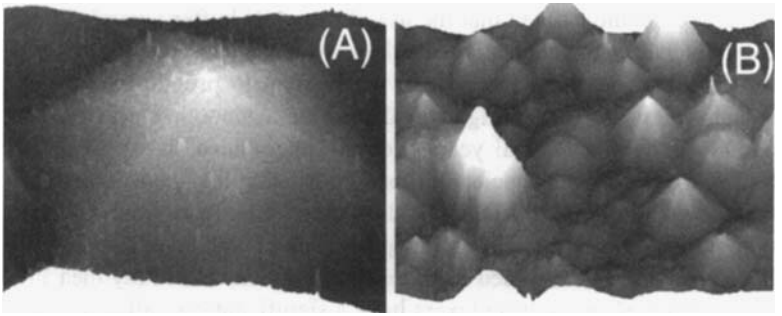


FIGURE 2 Atomic force microscopy images (100 μm × 100 μm) for unnucleated growth of GaN thin films in: (A) hydrogen as the carrier gas and (B) nitrogen as the carrier gas.

dimensions of only 10 to 20 μm and are 200 to 400 nm high. Even the crystallites that appear flat have a shallow pyramidal top. Here, the smaller subunits are 120 to 145 nm across and are more crystalline in appearance than those for unnucleated growth in hydrogen, and the prisms also appear to be less closely packed.

The pseudo-two-dimensional growth surfaces of the self-nucleated GaN films [Figs. 3 (A) and (B)] are expectedly smooth compared to those for the island growth mode of the unnucleated films. These self-nucleated films are, however, still composed of islands 8 to 10 μm across. A few of the islands give the appearance of being as large as 30 μm across, but these are more likely made up of clusters of smaller islands. The individual islands have steps as small as 0.3 to 0.4 nm and terraces of up to 150 to 300 nm across, depending on the region of the film scanned. In many cases the tops of the grains appear to end in a spiral; and in other cases some shallow holes are seen to be present, probably indicative of open-core screw dislocations. Even though the islands are not well faceted, the terraces do have straight edges, and the overall appearance of some of the islands is suggestive of the same 6-fold symmetry more obviously displayed by the large grains of the unnucleated films.

## X-Ray Scattering: Structural Coherence and Mosaic Dispersion

The out-of-plane structural coherence has been investigated by X-ray rocking curves for the (00.2)GaN reflection as illustrated in Fig. 4(A).[8]

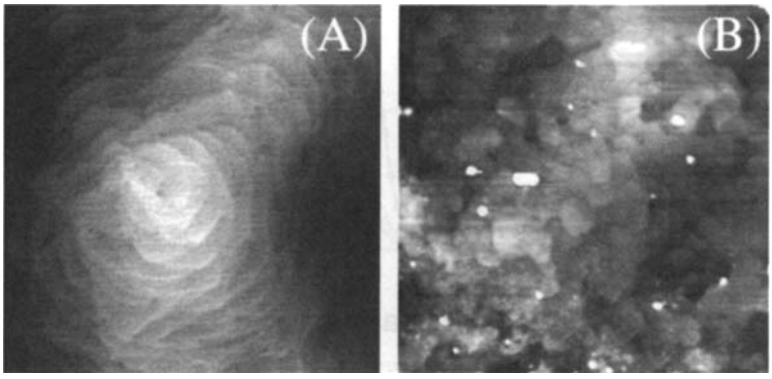


FIGURE 3 Atomic force microscopy images (4 μm × 4 μm) for: (A) self-nucleated growth of GaN thin films in hydrogen as the carrier gas and (B) self-nucleated growth of GaN thin films in nitrogen as the carrier gas.

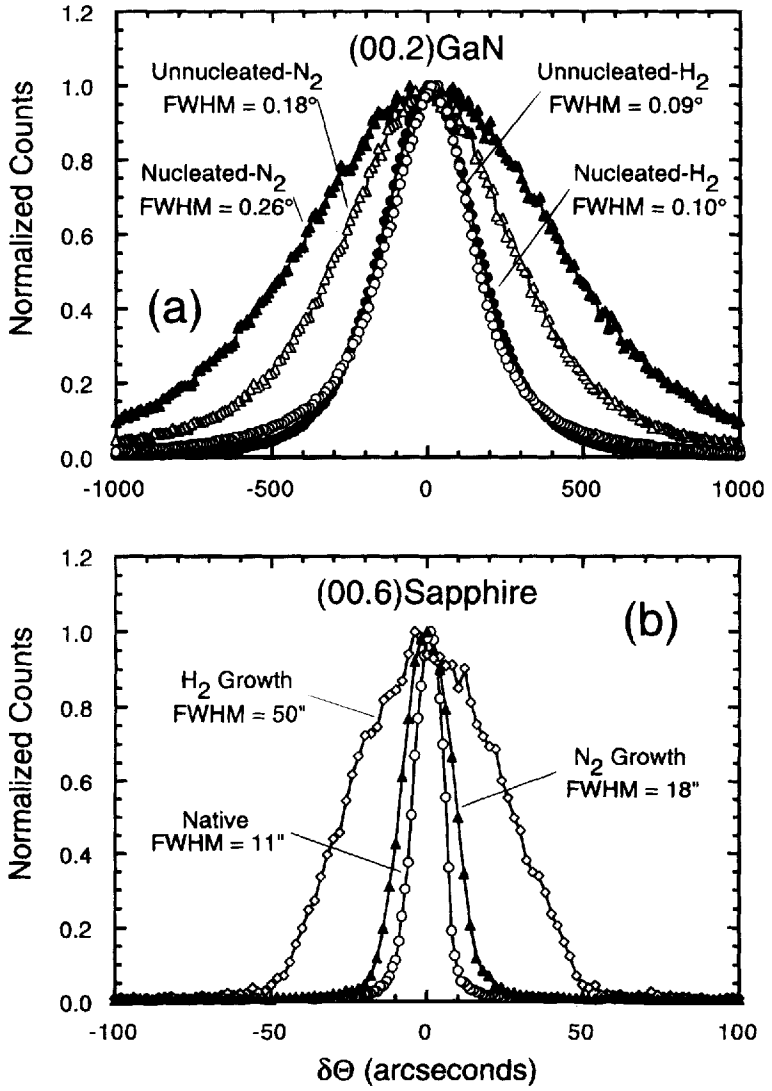


FIGURE 4 Comparison of X-ray rocking curves for: (A) the (00.2)GaN reflections from nucleated and unnucleated GaN films grown in hydrogen or nitrogen as the carrier gas and (B) the (00.6) reflections from the companion sapphire substrates.

Interestingly, these curves very clearly differentiate between films grown in nitrogen and hydrogen as the carrier gas. For both unnucleated and self-nucleated growth in hydrogen, the full-widths at half-maximum for the (00.2)GaN reflection are essentially identical at 0.10° (360 arcsec). In contrast, for growth in nitrogen, FWHM values near 0.2° are found for unnucleated films and even larger values, 0.25° to 0.45°, for self-nucleated films.

Finally, X-ray rocking curves for the (00.6) reflection from the sapphire substrate were also measured, and typical scans are shown in Fig. 4 (B). The rocking curve for the native (00.1) sapphire substrate shows an expectedly small FWHM of ~11 arcseconds, typical of a largely unstrained single-crystal substrate. As is indicated in Fig. 4, the inhomogeneous strain and resulting mosaic spread in the (00.1) sapphire substrate has measurably increased along the film growth direction when either nitrogen (~18 arcsec) or hydrogen (~50 arcsec) is employed as the carrier gas, the larger increases occurring for either nucleated or unnucleated growth in hydrogen.



Variations in the in-plane structural coherence were probed by measuring the X-ray scattering from {hh.0} reciprocal lattice vectors for both the thin films and the sapphire substrate by the X-ray precession method.[1,8] Zero-level precession photographs (Fig. 5) of the combined scattering from the (hh.0) reciprocal lattice planes of the (00.1) sapphire substrate and the (00.1) heteroepitaxial GaN film reveal the expected in-plane epitaxial relationship: $[\{10.0\}_{GaN}//\{11.0\}_{sapphire}]$. There is, moreover, a notable improvement in signal-to-noise ratio for growth in hydrogen, largely achieved by a reduction in noise. Several potential processes contribute to the background level, including: fluorescence; extrinsic instrumental scattering; and bremsstrahlung and diffuse scattering. While it might be expected that fluorescence and the extrinsic incoherent (Compton modified) fraction of the diffuse scattering are largely sample independent, the coherent scattering from various kinds of imperfections (point and line defects, stacking faults, surface roughness, and homogeneous and inhomogeneous stress) is expected to be sample dependent. Thus, the reduced background for growth in hydrogen as compared to nitrogen is likely due to a decrease in the density of such imperfections.

In that context, transmission electron microscopy studies have begun to appear for growth on a number of substrates using hydrogen as the carrier gas. In parallel, these studies have shown abrupt interfaces, a pre-

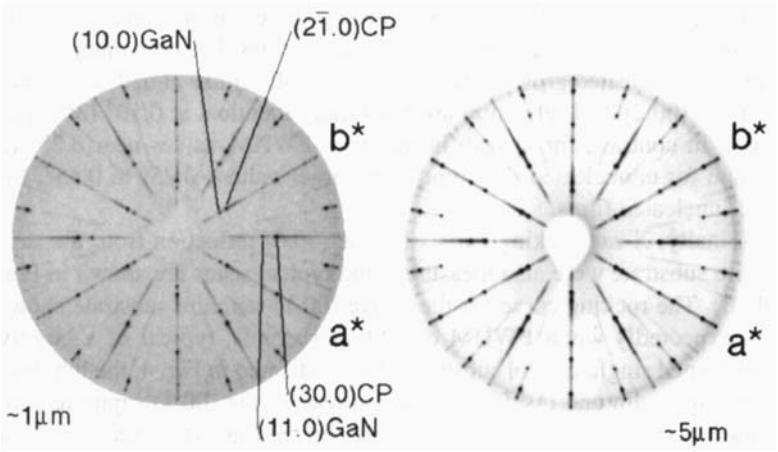


FIGURE 5 X-Ray precession photographs of the (hh.0) reciprocal lattice planes of (00.1)GaN on (00.1)sapphire for: (left) self-nucleated growth in a nitrogen and (right) self-nucleated growth in a hydrogen as the carrier gas.



dominance of (00.1) stacking faults, interfacial misfit dislocations (with densities of order $10^{10}$ $cm^{-2}$) and loops, and defect microstructure arising from island nucleation and coalescence. The implication from the X-ray precession study is that the defect densities could be even greater for growth in nitrogen as the carrier gas.

### $Al_xGa_{1-x}N$ Thin Films

Solid solutions in the Al–Ga–N system were first reported in 1973,[9] and single-crystal quality layers of $Al_xGa_{1-x}N$ were grown by vapor phase epitaxy on sapphire in 1978.[10] However, few comprehensive studies have been undertaken, and there remains some controversy as to fundamental properties, particularly the determination of the sign and magnitude of the bowing parameter $b$—a measure of the intrinsic (change in lattice parameter) and extrinsic (substitutional disorder) inhomogeneities in the crystal potential. The early observations were collected on samples deposited directly onto the substrate. As noted earlier, thin buffer layers of either AlN or GaN greatly improve the crystallographic, electrical, and optical properties of GaN and $Al_xGa_{1-x}N$ alloy films.

Alloy compositions ($x$) as determined by energy-dispersive X-ray spectroscopy and by X-ray diffraction measurement of the lattice constants agreed to within ±0.02, confirming that Vegard's law is obeyed for these self-nucleated $Al_xGa_{1-x}N$ films. The high crystalline quality of these $Al_xGa_{1-x}N$ alloy films is evidenced by $\theta/2\theta$ X-ray diffractometer scans.[11] As for GaN, the (00.1) plane of the $Al_xGa_{1-x}N$ layer parallels that of the sapphire substrate, and the clear separation in the $K\alpha_1/K\alpha_2$ doublets for the low-angle (00.2) reflection show that the structural coherence parallel to the growth direction is excellent. The full-width at half-maximum from a Lorentzian fit to the $K\alpha_1$ component as a function of alloy composition increases mildly with increasing alloy composition, implying minimal increases in physical and chemical inhomogeneity on alloying. Using the X-ray precession method, the quality of the in-plane heteroepitaxy [as now expected $\{10.0\}_{Al_xGa_{1-x}N}$// $\{11.0\}_{sapphire}$] has also been assessed as a function of alloy composition. In line with the trend in the **c**-axis length, the **a**-axis length varies linearly with composition, with a gradient correlating with the different **c/a** ratios of GaN and AlN. Furthermore, the azimuthal coherence (mosaic spread) deteriorates slightly across the series, presumably in parallel with the softly degraded structural coherence seen in the film growth direction.

In order to assess the misorientation of the mosaic of $Al_xGa_{1-x}N$ islands relative to the growth direction (polar dispersion), X-ray rocking curves through this same (00.2) reciprocal lattice vector have been recorded,[12] and Fig. 6 displays rocking curves for films with compositions ranging from $x = 0$ (GaN) to $x = 0.38$. Three features of the scattering profiles are immediately evident: (1) there is a shift to higher $\theta$ with increasing $x$ that reflects the decreasing (linearly) **c** cell constant; (2) the peak widths are on the order of tenths of a degree and are much larger than that for the comparable (00.6) reflection from the sapphire substrate; and, (3) there is a systematic broadening of the full-width at half-maximum for the X-ray rocking curve with increasing Al content, signaling a decrease in orientational coherence. Specifically, the variation in the FWHM as a function of film composition is shown in Fig. 7(a) and displays a clear linear dependence, with the FWHM nearly doubling on going from $x = 0$ to $x = 0.38$.[12]

We next turn to the optical characteristics of these alloy films, and Fig. 8 shows a plot of the square of the absorption coefficient $\alpha$ as a function of photon energy for a selection of $Al_xGa_{1-x}N$ alloys in the

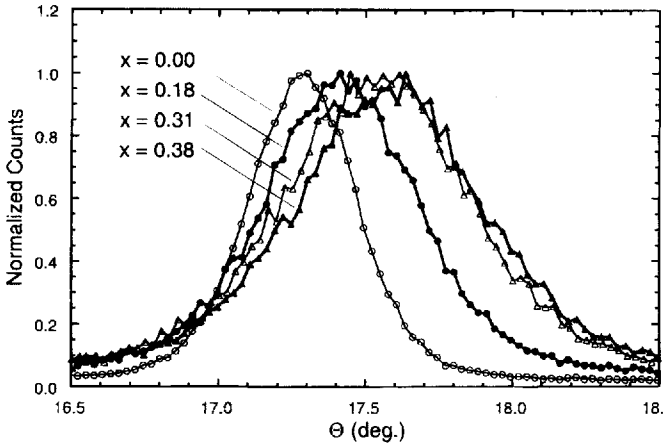


FIGURE 6 X-Ray rocking curves through the (00.2) reflection for several $Al_xGa_{1-x}N$ thin films. The shift to larger θ along the abscissa reflects the decrease in the c cell constant with increasing Al concentration.



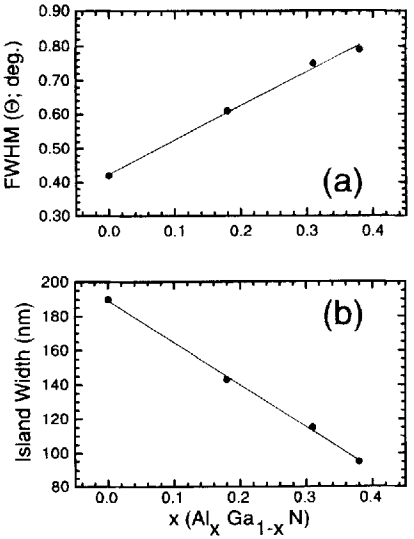


FIGURE 7 Variation as a function of film composition for: (a) the FWHM for the X-ray rocking curve of the (00.2)$Al_xGa_{1-x}N$ reflection; (b) island width.

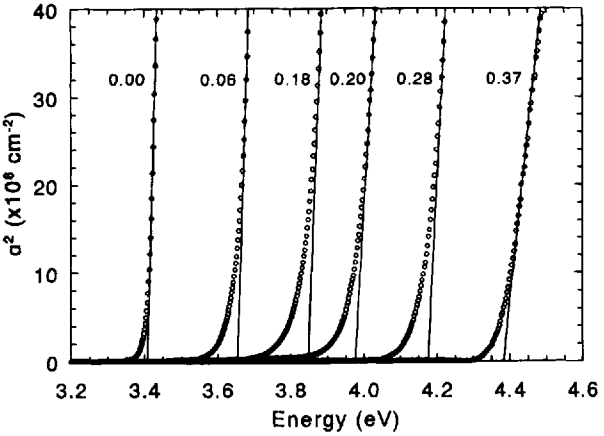


FIGURE 8 Absorption coefficient squared ($\alpha^2$) as functions of photon energy for $Al_xGa_{1-x}N$ alloys with $x < 0.4$.



range $0 \leq \times \leq 0.4$.[11] The solid lines are drawn from the point of maximum gradient in the absorption curves, and their extrapolated intercepts were used to calculate the optical bandgap energies $E_g$ of these $Al_xGa_{1-x}N$ alloys. The absorption curves do not exhibit the large low energy tails observed in some other studies, indicating once again that there are minimal macroscopic non-uniformities in the samples. In fact, probing the films with a 1 mm diameter beam aperture showed a variation of less than ±0.02 eV in the derived $E_g$, corresponding to a variation in $x$ of less than 0.01.

Finally, a plot of the optical bandgap energy $E_g$ as a function of the alloy composition is given in Fig. 9 and shows a nominally linear dependence of $E_g$ on $x$ with the bowing parameter $b \approx 0$ eV. This is in disagreement with samples deposited both directly onto sapphire and onto AlN-buffered sapphire substrates. The magnitude of this discrepancy is illustrated in Fig. 9 by the dashed lines representing the reported range of $b$ values. It is difficult to fully resolve these differences, although it is noted that both the lattice constant and energy gap of a particular $Al_xGa_{1-x}N$ film are functions of any residual strain present. It has been shown that GaN nucleation layers deposited on (00.1) sapphire substrates become fully relaxed by the time that they have been ramped from their deposition temperature to the growth temperature of the GaN overlayer, a result that is independent of film thickness.[7] It has been

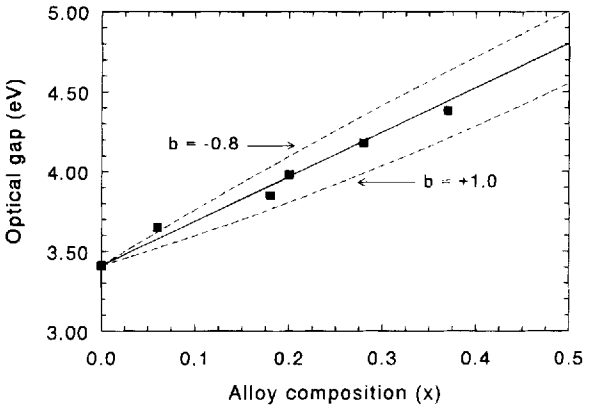


FIGURE 9 Optical energy gap of $Al_xGa_{1-x}N$ layers as function of alloy composition $x$. The solid line represents bowing parameter $b = 0$; the dashed lines represent the range of $b$ values reported in the literature.



speculated[12] that the differing results for the trends in optical bandgaps are attributed to an equal variance in the residual strain.

## Scanning Tunneling Microscopy: Surface Imaging

Representative scanning tunneling microscopy (STM) scans for four $Al_xGa_{1-x}N$ thin films are displayed in Fig. 10. It is immediately discernible that on a fine scale these films are also comprised of a dense mosaic of highly oriented grains, with disk-like features yielding surface height modulations of 1–2 nm and average island diameters on the order of a few hundred nanometers. It is further apparent that there is a significant decrease in island size with increasing Al concentration. In fact, the decrease in island width from STM or AFM scans is also linearly correlated with film composition as depicted in Fig. 7(b). Furthermore, over the compositional range spanned by these films, the relative rate of decrease (about a factor of 2) in in-plane island width is nearly the same as the relative rate of increase in the out-of-plane misorientation (inversely proportional to the FWHM) [Fig. 7(a)]. It seems clear, then, that these two structural properties are highly correlated.

The decrease in grain size in these self-nucleated $Al_xGa_{1-x}N$ alloy films implies a parallel reduction in a growth factor influenced by increasing Al content. This has also been observed across a series of

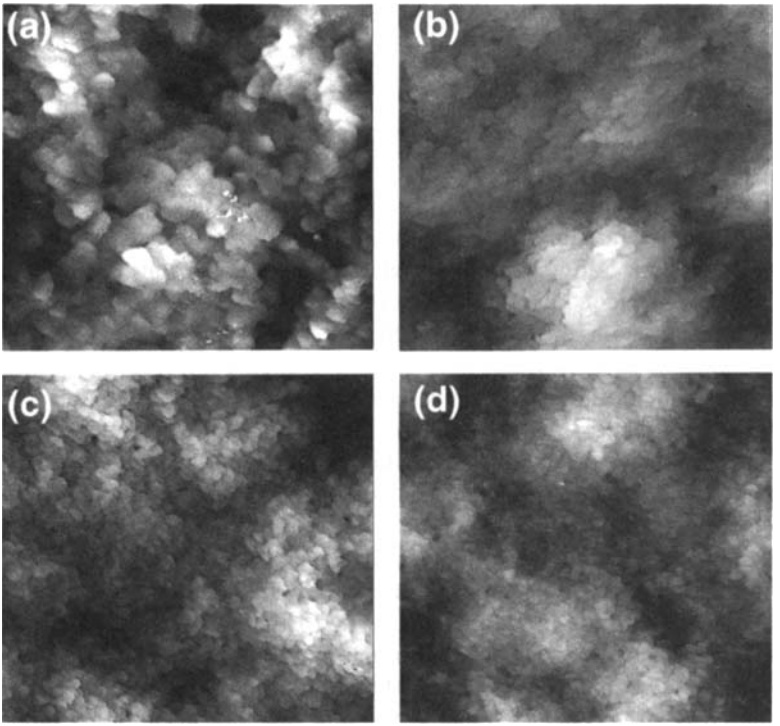


FIGURE 10 Scanning tunneling microscopy images (4μ × 4μ) for $Al_xGa_{1-x}N$ thin films with: (a) $x = 0$; (b) $x = 0.18$; (c) $x = 0.31$; and (d) $x = 0.38$.



AlN-nucleated films,[13] where there is a common nucleation layer whose lattice mismatch with the overlayer decreases with increasing Al content. It might have been anticipated in this latter case that the grain size could in fact increase with increasing $x$ (in contrast to experiment). In the self-nucleated films, the nucleation layer composition matches that of the overlayer and could lead to the naive speculation that the grain size might remain essentially constant (again in contrast to experiment). The accumulated results suggest, then, that lattice matching the nucleation layer and overlayer is not a predominant factor in modifying the growth mode, although the reduction in grain size with increasing Al content is considerably less pronounced for the self-nucleated films. What the comparison of the results of these two studies does is to demonstrate that a reduction in surface mobility or nucleation site den-

sity with increasing Al content dominates the growth process for the $Al_xGa_{1-x}N$ overlayers.

## CONCLUSIONS AND PROSPECTIVE APPLICATIONS

The improvements in growth and characteristics of GaN and $Al_xGa_{1-x}N$ thin films have resulted in significant inroads in device technology.[14,15] For example, high-efficiency blue-emitting metal-insulator-semiconductor light-emitting diodes (LEDs) have been fabricated and, with the advent of Mg-doped *p*-type material, violet emitting *pn*-junction LEDs have been developed. Prototype GaN metal semiconductor field-effect transistors have also been reported. In addition, high-quality, low-aluminum-content $GaN/Al_xGa_{1-x}N$ heterostructures have been produced that exhibit quantum confinement effects by photoluminescence, stimulated emission under photon pumping, and electron mobility enhancement. In addition, violet-emitting indium gallium nitride ($In_{1-x}Ga_xN$)/GaN LEDs with external quantum efficiencies of 0.22% have been developed and double-heterostructure blue- and green-emitting $In_{1-x}Ga_xN/Al_yGa_{1-y}N$ LEDs with external quantum efficiencies of over 6% have been reported.[16] For ourselves, we have concentrated on the development of solar-blind UV detectors based on the $Al_xGa_{1-x}N$ system.[17] Finally, the long-sought nitride-based blue-laser diode has recently been achieved.[18]

These results demonstrate that GaN and its alloys can no longer be regarded as "semiconductors of the future," particularly since $In_{1-x}Ga_xN/Al_yGa_{1-y}N$ thin-film devices are currently under full-scale production. However, it is apparent that the crystal quality and defect density of even the best heteroepitaxial GaN material is far from ideal and that much work still remains to be undertaken before the system can be considered fully under technological control.



**Acknowledgments**

The authors gratefully acknowledge a number of colleagues (especially W. A. Bryden, J. A. Miragliotta, S. A. Ecelberger, and C. B. Bargeron from Johns Hopkins, M. E. Hawley from Los Alamos National Laboratory, and R. P. Leavitt from the Army Research Laboratory, Adelphi), who have been instrumental in much of the research reported on here.

We also acknowledge several sponsors (including the Department of the Navy and the National Aeronautics and Space Administration) for their continued support of this program.

## References

1. T. J. Kistenmacher, W. A. Bryden, J. S. Morgan and T. O. Poehler, J. Appl. Phys. **68**, 1541 (1990).
2. H. M. Manasevit and W. I. Simpson, J. Electrochem. Soc. **116**, 1725 (1969).
3. E. G. Bauer *et al.*, J. Mater. Res. **5**, 852 (1990).
4. H. Amano, N. Sawaki, I. Akasaki and Y. Toyoda, Appl. Phys. Lett. **48**, 353 (1986).
5. D. K. Wickenden, T. J. Kistenmacher, W. A. Bryden, J. S. Morgan and A. Estes Wickenden, Mat. Res. Soc. Symp. Proc. **221**, 167 (1991).
6. S. Nakamura, Jpn. J. Appl. Phys. **30**, L1705 (1991).
7. A. Estes Wickenden, D. K. Wickenden and T. J. Kistenmacher, J. Appl. Phys. **65**, 5367 (1994).
8. T. J. Kistenmacher, D. K. Wickenden, M. E. Hawley and R. P. Leavitt, Mat. Res. Soc. Symp. Proc., in press.
9. M. D. Lyutaya and T. S. Bartnitskaya, Inorg. Mater. **9**, 1052 (1973).
10. J. Hagen, R. D. Metcalf, D. K. Wickenden and W. Clark, J. Phys. C **11**, L143 (1978).
11. D. K. Wickenden, C. B. Bargeron, W. A. Bryden, J. Miragliotta and T. J. Kistenmacher, Appl. Phys. Lett. **65**, 2024 (1994).
12. T. J. Kistenmacher, D. K. Wickenden, M. E. Hawley and R. P. Leavitt, Appl. Phys. Lett. **67**, 3771 (1995).
13. Y. Koide, H. Itoh, N. Sawaki, I. Akasaki and M. Hashimoto, J. Electrochem. Soc. **133**, 1956 (1986).
14. S. Strite and H. Morkoc, J. Vac. Sci. Technol. **10**, 1237 (1992).
15. S. N. Mohammad, A. A. Salvadore and H. Morkoc, Proc. IEEE **83**, 1306 (1995).
16. S. Nakamura, M. Senoh, N. Iwasa, S. Nagahama, T. Yamada and T. Mukai, Jpn. J. Appl. Phys. **34**, L1332 (1995).
17. D. K. Wickenden, W. A. Bryden, T. J. Kistenmacher, P. F. Bythrow and K. Strohbehn, Johns Hopkins APL Technical Digest **16**, 246 (1995).
18. S. Nakamura *et al.*, Jpn. J. Appl. Phys. **35**, L74 (1996).